

Coherent confinement and unidirectional dynamics of a wave packet induced by a non-Hermitian Su-Schrieffer-Heeger segment

K. L. Zhang and Z. Song*

School of Physics, Nankai University, Tianjin 300071, China

The competition between staggered imaginary potentials and lattice dimerization results in a unidirectional propagating coalescing state of a non-Hermitian Su-Schrieffer-Heeger (SSH) ring at an exceptional point. A segment of the SSH ring inherits the unidirectional feature and exhibits some intriguing dynamic behaviors when it is embedded in a Hermitian chain as a \mathcal{PT} -symmetric scattering center. Based on the Bethe ansatz scattering solution for the interface between Hermitian and non-Hermitian regions, we show that the SSH scattering center supports the following wave-packet dynamics. (i) A left incident wave packet is allowed perfect transmission, while a right incident wave packet stimulates an amplified reflecting wave train with the length proportional to the size of the SSH segment. Accordingly, a unidirectional invisibility of Bragg scatterers is observed when a multi-SSH segment is considered. (ii) A left incident wave packet can be well confined in a SSH segment if the right lead is removed. (iii) In addition, a wave packet is perfectly absorbed when its size closes to the length of the SSH segment. The underlying mechanism stems from a subtle property of the SSH segment, which supports two quasicolescing wave packets but with opposite group velocities. Our findings are applicable to the schemes of realizing quantum state storage, quantum diode, and lasing device.

I. INTRODUCTION

The introduction of complex potential in a Hamiltonian extends the frontier of conventional quantum mechanics. Non-Hermitian systems make many things possible including unidirectional propagation and anomalous transport [1–8], invisible defects [9–11], coherent absorption [12] and self sustained emission [13–17], loss-induced revival of lasing [18], as well as laser-mode selection [19, 20]. Such kinds of novel phenomena can be traced to the existence of exceptional point (EP). On the other hand, implementing the tasks of quantum information processing via non-Hermitian systems becomes an attractive topic. Recently, critical behavior of non-Hermitian system has been employed to generate entangled states in a dynamical process [21–24]. It is well known that a static Hamiltonian cannot realize a coherent confinement of a wavepacket in the framework of Hermitian quantum mechanics, which is a key ingredient for the storage of quantum information. It is always implemented by time-dependent system [25–28], employing adiabatic or diabatic dynamical process. It seem impossible to stop and confine a wavepacket via a natural time evolution under an always-on Hermitian system. As illustrated in Figs. 1(a) and (c), a wave packet can be transferred from certain location to a confining region by a natural time evolution. This process can be achieved by a time-independent Hermitian Hamiltonian. In order to confine the wave packet, a time-dependent term should be added (Fig. 1(b)). A simplest way is to switch off the tunneling channel at way out. However, it may be done by a natural time evolution under a time-independent non-Hermitian Hamiltonian (Fig. 1(d)) since a non-Hermitian system

exhibits strong unidirectional dynamics [17, 29–36]. It is expected that a wavepacket can perfectly come in the confining region without any reflection, but do not leak out from the region. In addition, a compound system that consists of non-Hermitian and Hermitian segments, such as a sandwich structure, may possess some unrevealed features to be explored.

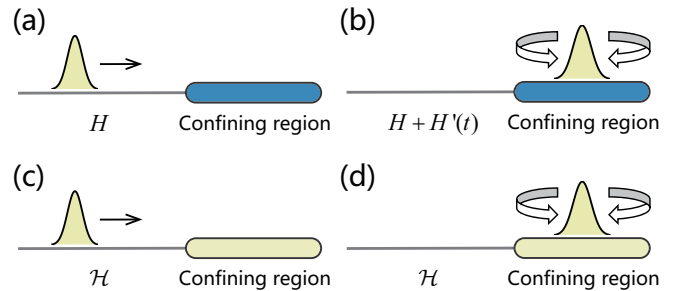


FIG. 1. Schematic illustration of the coherent confinement. (a) and (b) is the time-dependent Hermitian system; (c) and (d) is the time-independent non-Hermitian system.

In this paper, we consider whether it is possible to use time-independent non-Hermitian systems to realize a coherent confinement of wavepacket via natural time evolution. We investigate the scattering problem of the interface between a uniform Hermitian and non-Hermitian Su-Schrieffer-Heeger (SSH)-type semi-infinite chains via Bethe ansatz technique. It describes a junction of two types of materials, Hermitian and non-Hermitian, which have different properties. The essence is that the competition between staggered imaginary potentials and lattice dimerization in a SSH model result in a unidirectional propagating coalescing state at EP. And a segment of the SSH ring inherits the unidirectional feature and exhibits some intriguing dynamic behaviors when it is embedded

* songtc@nankai.edu.cn

in a Hermitian chain as a \mathcal{PT} -symmetric scattering center (sandwich). Analytical and numerical results indicate that a SSH scattering center supports the following wave packet dynamics: (i) A left incident wave packet is allowed perfect transmission, while a right incident wave packet stimulates an amplified reflecting wave train with the length proportional to the size of the SSH segment. A unidirectional invisibility of Bragg scatterers is observed when multi-embedded-SSH-segment is considered. (ii) A left incident wave packet can be well confined in SSH segment if the right lead is removed. (iii) In addition, a wave packet is perfectly absorbed when its size closes to the length of the SSH segment. The underlying mechanism relates to the peculiar dynamics of wave packet at EP. Two wave packets with maximal opposite group velocities can cancel each other out due to the fact that the main components of two wave packets are the same coalescing state. In contrast, two similar wave packets for Hermitian uniform chain are always orthogonal in the context of Dirac inner product. The proposed schemes do not require complicated structure, which is accessible in optical system. Our findings are applicable to the schemes of realizing quantum state storage, quantum diode and lasing device.

This paper is organized as follows. In Sec. II, we present the model consisted of two semi-infinite chains and the scattering solutions at the interface. In Sec. III, we discuss the dynamics of the system with the non-Hermitian SSH segment as a scattering center. In Sec. IV, we demonstrate the coherent confinement and perfectly absorbed dynamics of the semi-infinite system. In Sec. V, we summarize our findings.

II. SCATTERING AT INTERFACE

One of the exclusive features of a non-Hermitian system is the unidirectional dynamical behavior, which cannot occur in a Hermitian system even the parity symmetry is broken. For instance, a non-Hermitian SSH chain, the competition between staggered imaginary potentials and lattice dimerization result in a unidirectional propagating coalescing state at EP [36, 37], while a linear field breaks the isotropy of a uniform Hermitian chain in both directions, but can only lead to a Bloch oscillation, exhibiting reversibility of wavepacket dynamics [38, 39]. An interesting question is what happens when such two systems are jointed together to form an infinite chain. Figures 2(a) and (b) are the schematic illustrations of this configuration. In the following, we will investigate the scattering solution for such an interface, which is expected to shed light on the property of the interface between a Hermitian and non-Hermitian system in general.

The corresponding Hamiltonian reads

$$\mathcal{H} = H_{\text{I}} + H_{\text{II}}, \quad (1)$$

which is consist of two semi-infinite chains. Here H_{I} de-

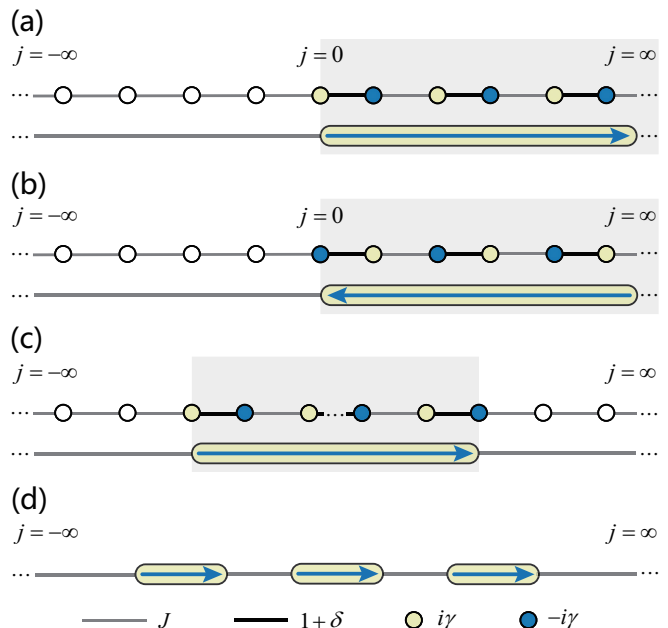


FIG. 2. Schematic illustration of the non-Hermitian infinite chain representing by Eq. (1), which is consist of semi-infinite subsystems: The uniform chain and the non-Hermitian SSH chain. (a) The uniform chain is connected to the gain site of the non-Hermitian SSH chain. (b) The uniform chain is connected to the loss site of the non-Hermitian SSH chain. (c) A finite non-Hermitian SSH segment embedded in a uniform chain as a \mathcal{PT} -symmetric scattering center. (d) A multi-layer sandwich structure, in which many SSH segments are embedded in a uniform chain. The gray line and blue arrow represent the uniform chain and non-Hermitian SSH chain, respectively.

scribes a Hermitian uniform semi-infinite chain

$$H_{\text{I}} = J \sum_{j=-\infty}^{-1} a_j^\dagger a_{j+1} + \text{H.c.}, \quad (2)$$

and H_{II} is a non-Hermitian semi-infinite SSH chain

$$H_{\text{II}} = \sum_{l=0}^{\infty} [(1 + \delta) a_{2l}^\dagger a_{2l+1} + J a_{2l+1}^\dagger a_{2l+2} + \text{H.c.} + i\gamma(a_{2l}^\dagger a_{2l} - a_{2l+1}^\dagger a_{2l+1})], \quad (3)$$

where a_j and a_j^\dagger are particle operators of fermion or boson. The interface of the Hermitian and non-Hermitian regions is at $j = 0$. We notice that \mathcal{H} breaks the time reversal symmetry and $\mathcal{H}(\gamma) = \mathcal{H}^*(-\gamma) = \mathcal{H}^\dagger(-\gamma)$. In this paper, we focus on the situation with the parameter satisfying $\gamma = \pm(1 + \delta - J)$, which are shown in Figs. 2(a) and (b). Before we deal with the solution of \mathcal{H} , we briefly review the features of solutions of H_{I} and H_{II} on an N -site ring lattice, which indicate the motivation of the above parameter setting.

For the uniform ring, H_{I} supports two degenerate zero modes in the form of $|\psi_{\pm}\rangle = N^{-1/2} \sum_{j=1}^N e^{\pm i(\pi/2)j} |j\rangle$.

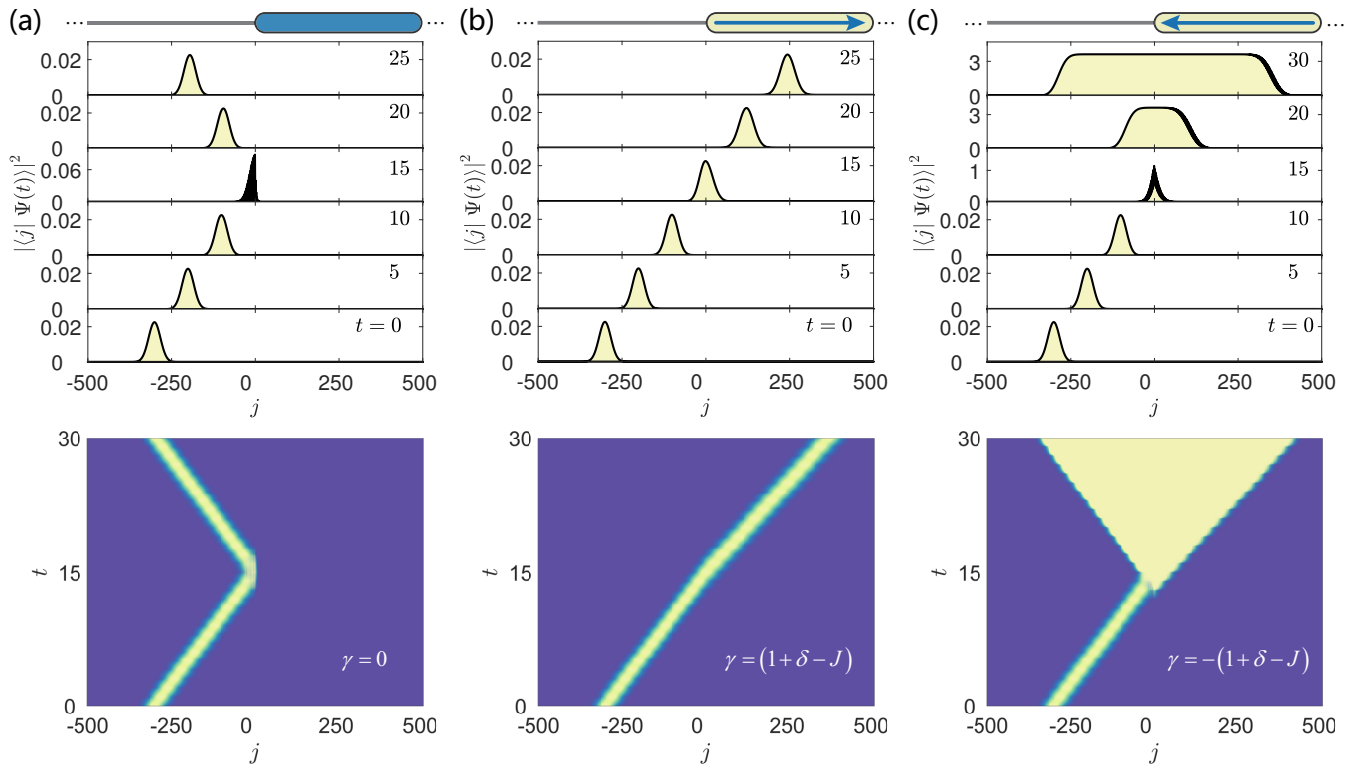


FIG. 3. Numerical simulations of the dynamics for three typical situations. The system is consist of a uniform chain and a SSH chain. (a) Dynamics of perfect reflection for the Hermitian lattice, which is consist of a uniform chain and a Hermitian SSH chain. (b) Perfect transmission without reflection for the system in Fig. 1(a). (c) Amplified transmission and reflection for the system in Fig. 1(b). The parameters of the initial excitation are $\alpha = 0.04$, $N_c = -300$ and $k_c = -\pi/2$. The parameters of the system are $J = 1$, $\delta = 0.5$ and $\gamma = 0$ for (a); $\gamma = 0.5$ for (b); $\gamma = -0.5$ for (c). The time unit is $10J^{-1}$.

Obviously, both directions are symmetric. The corresponding ring system for non-Hermitian H_{II} is at EP when takes $\gamma = \pm(1 + \delta - J)$. It supports a single coalescing zero-energy eigenstate: $|\psi_+\rangle$ or $|\psi_-\rangle$, depending on the parameter $\gamma = \pm(1 + \delta - J)$, which exhibits strongly unidirectionality. Thus, it is expected that the infinite system \mathcal{H} support a zero energy scattering wave function $\sum_{j=-\infty}^{\infty} e^{-i\frac{\pi}{2}j} |j\rangle$ or $\sum_{j=-\infty}^{\infty} e^{i\frac{\pi}{2}j} |j\rangle$, corresponding to the parameter $\gamma = (1 + \delta - J)$ or $\gamma = -(1 + \delta - J)$, respectively. Furthermore, it has been shown that H_{II} still has many intriguing features, such as simple harmonic oscillation and position-independent lasing [37, 40], even for the open boundary condition. The underlying mechanism of these phenomena, that is also the heart of this work, is the unidirectionality inherited from the SSH ring at EP.

Now we turn to the combination of such two systems, by solving the scattering problem of the interface between Hermitian and non-Hermitian regions as the scattering center. In general, the ansatz wave function in single-particle subspace has the form

$$|\psi\rangle = \sum_{j=-\infty}^{\infty} f_j |j\rangle, \quad (4)$$

with

$$f_j = \begin{cases} \mathcal{I}e^{iKj} + \mathcal{O}e^{-iKj}, & j < 0 \\ \mathcal{I}^A e^{-ikj} + \mathcal{O}^A e^{ikj}, & j = 2l \\ \mathcal{I}^B e^{-ikj} + \mathcal{O}^B e^{ikj}, & j = 2l + 1 \end{cases}. \quad (5)$$

For simplicity, we focus on the system with parameter $\gamma = \pm(1 + \delta - J)$ and the solutions with zero energy. The solution of scattering wave function can be obtained by the Bethe ansatz method (see Appendix A).

For the case with $\gamma = (1 + \delta - J)$, it is shown that the scattering solution is

$$|\psi\rangle = \sum_{j=-\infty}^{\infty} e^{-i\frac{\pi}{2}j} |j\rangle, \quad (6)$$

which is a plane wave, supporting the perfect transmission without reflection for the wave packet with momentum center $\pi/2$. It means that the wave packet propagates with Dirac probability preservation and without shape deformation. However, for $\gamma = -(1 + \delta - J)$, the scattering solution is

$$|\tilde{\psi}\rangle = \sum_{j=-\infty}^{\infty} e^{i\frac{\pi}{2}j} |j\rangle, \quad (7)$$

which can be obtained by directly applying the time-reversal operator on the system and the solution. We list the two solutions explicitly for the use of constructing the scattering solution for a non-Hermitian SSH segment as a scattering center.

The above two solutions indicate the unidirectionality of the system, which is arisen from the non-Hermitian part of the system in Eq. (3), i.e., the competition between staggered imaginary potentials and lattice dimerization. In general, a plane wave solution can be utilized to predict the wave packet dynamics. To demonstrate this feature, we perform the numerical simulation of the time evolution for an initial Gaussian wave packet

$$|\Psi(0)\rangle = \Omega^{-1/2} \sum_{j=-\infty}^{\infty} e^{-\alpha^2(j-N_c)^2/2} e^{ik_c j} |j\rangle, \quad (8)$$

where N_c is the wave packet center, k_c is the central momentum, and $\Omega = \sqrt{\pi}/\alpha$ is the normalization factor. The evolved state obeys the equation $|\Psi(t)\rangle = e^{-i\mathcal{H}t} |\Psi(0)\rangle$, which can be computed by exact diagonalization of a finite system with sufficient large size. As comparison, we focus on three cases with $\gamma = 0$ and $\gamma = \pm(1 + \delta - J)$. The numerical results for three typical situations are shown in Fig. 3. For the system in Fig. 2(b), the scattering solution corresponding to an incident plane wave with momentum $-\pi/2$ incoming from the left of system can not be obtained through the scattering theory for plane waves. The dynamics for perfect transmission without reflection in Fig. 3(b) accords with the previous analysis. In Fig. 3(c), we can see that for the system in Fig. 2(b), an incident plane wave incoming from the left of the system gives rise to amplified transmission and reflection. So far, the mechanism of this behavior is unclear, but it is not the focus of the present work. The dynamics of wavepacket for non-Hermitian system in Figs. 3(b) and (c) can not be seen in a Hermitian system in Fig. 3(a), which is consist of a uniform chain and a Hermitian SSH chain by taking $\gamma = 0$. In this Hermitian system, the energy levels of the uniform chain does not match the one of the Hermitian SSH chain, i.e., the plane wave mode with momentum $\pm\pi/2$ is forbidden due to the energy gap of the Hermitian SSH chain. Thus the wave packet cannot pass through the interface of two chains, exhibiting the perfect reflection.

III. NON-HERMITIAN SSH-SEGMENT SCATTERING CENTER

In Sec. II, we have discussed the scattering features at the interface of Hermitian uniform chain and non-Hermitian SSH chain in specific case. Both the Hermitian and non-Hermitian systems are semi-infinite. It reveals the unidirectional feature of non-Hermitian SSH model. In this section, we consider the case with a finite non-Hermitian SSH segment embedded in a uniform chain as a \mathcal{PT} -symmetric scattering center. Schematics of such a

system is given in Fig. 2(c). A solution of such a sandwich can be obtained by the combination of Eqs. (6) and (7), when the number of sites of the non-Hermitian SSH segment is even Δ , which ensures the balance of gain and loss. Furthermore, such a resonant transmission solution can be extended to a multi-layer sandwich structure, in which many SSH segments are embedded in a uniform chain (see Fig. 2(d)).

This feature can be demonstrated via wave packet dynamics. We perform the numerical simulation for the time evolution of Gaussian wave packets with two initial situations. The numerical results for the wave packet incoming from the left and the right of the system are shown in Figs. 4(a) and (b), respectively. In Fig. 4(a), we can see that the left-incident wave packet pass through the non-Hermitian SSH segment without reflection, and the probability is conserved. This accords with the prediction from Bethe ansatz solution. Actually, in certain non-Hermitian systems, the dynamics of probability preservation can be realized when the initial states are structured properly, as shown in the previous works [40–43]. In Appendix C, we show that when the initial states are structured properly in a solvable non-Hermitian SSH ring, the Dirac probability conserve. Thus, together with the Bethe ansatz solution and the analysis in Appendix C, it is presumable that when certain type of wavepacket pass through the interface and evolve in a non-Hermitian SSH segment, the dynamics of probability preservation can be observed. In Fig. 4(b), we can see that the right-incident wave packet can trigger the full transmission associating with amplified reflecting wave train. The width of the amplified wave train h is about twice as the size of the non-Hermitian SSH segment: $h \approx 2\Delta = 300$. So for, this observation cannot be explained by the present scattering solution. We leave this issue for the future consideration.

The behavior of perfect transmission in Fig. 4(a) can be well understood. In Sec. II, we have discussed the scattering solutions for the systems in Figs. 2(a) and (b). And the sandwich structure in upper panel of Fig. 4(a) can be regarded as the combination of two system in Figs. 2(a) and (b), thus the scattering solutions in Eqs. (6) and (7) can explain the dynamics of perfect transmission in Fig. 4(a). Accordingly, a perfect transmission in multi-layer sandwich structure can be predicted by repeating the process in Fig. 4(a). In Figs. 4(c) and (d), numerical results for a Bragg-stack-like scattering center are plotted, which is similar to the experimental observation for unidirectional invisibility of \mathcal{PT} -symmetric Bragg scatterers [4].

IV. COHERENT CONFINEMENT AND PERFECT ABSORPTION

Before proceeding with this section we would like to reveal a peculiar feature of wave packet dynamics in a non-Hermitian SSH system at EP, which is crucial for

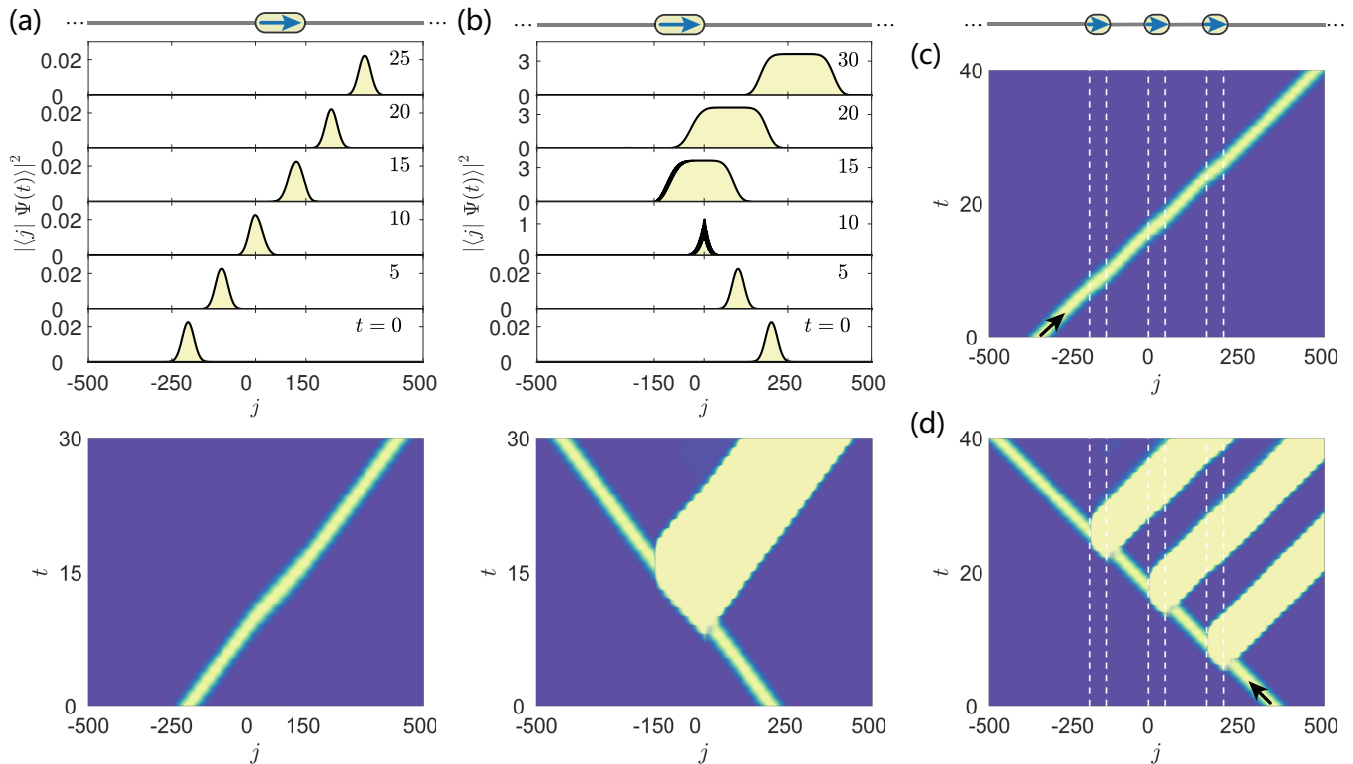


FIG. 4. Numerical simulations of the dynamics for the coupled system, which is from by a uniform chain embedded with a non-Hermitian SSH segment. (a) Perfect transmission without reflection. (b) Amplified reflecting wave train. The parameters of the initial excitation are $\alpha = 0.04$, $N_c = -200$ and $k_c = -\pi/2$ for (a); $\alpha = 0.04$, $N_c = 200$ and $k_c = \pi/2$ for (b). The length of the segment is $\Delta = 150$. (c) and (d) Numerical results for the Bragg-stack-like scattering center with initial Gaussian wave packet incoming from left and right of the system, respectively. The length of three segments are all $\Delta = 50$. Other parameters are $J = 1$, $\delta = 0.5$ and $\gamma = 0.5$. The time unit is $10J^{-1}$.

the mechanism of the phenomena that will be presented in this section. We start with the dispersion relation of the SSH model, which determines the group velocity of a wave packet. The dispersion relation is expressed as

$$\varepsilon_k^\pm = \pm \sqrt{J^2 + (1 + \delta)^2 - 2J(1 + \delta) \cos k} - \gamma^2, \quad (9)$$

which is plotted in Fig. 5(a) for several typical values of γ . We are interested in the case with $\gamma = 0.5$, at which a coalescing state appears at $k = 0$. In the vicinity of zero k , the dispersion relation is two crossing lines with the crossing point at EP. One can construct two wave packets ($|\psi_L\rangle$ and $|\psi_R\rangle$) as the form in Eq. (8) with zero energy, but with opposite group velocities, which correspond to the slopes of the linear dispersion lines. According to the analysis in Appendix D, there exist two quasi-coalescing sets of energy levels near the zero point. On the other hand, one can do the same thing for a Hermitian uniform chain (or the SSH model with $\gamma = \delta = 0$). However, two situations are different: (i) The zero point of the dispersion relation for the later is degenerate point; (ii) The two wave packets for the later are always orthogonal, while two wave packets in the non-Hermitian system have nonzero overlap in the context of Dirac inner product. In Fig. 5(b) we plot the profiles of two

wave packets in k space and real space. We get the conclusion that when two such wave packets meet together, the evolved state is a single wave packet with an additional overall factor $1 + e^{i\varphi}$. They can cancel out each other for $\varphi = \pi$, or double the amplitude for $\varphi = 0$. To demonstrate this results, numerical simulation is performed and the results are plotted in Figs. 5(c) and (d). The motivation of this study stems from the following paradox. (On the one hand,) an infinite SSH chain supports a $\pi/2$ plane wave, while a zero-energy solution is forbidden for a semi-infinite SSH chain (see Appendix B). The above analysis about the zero-energy wave packets indicates that the physics of the forbidden mode is the long-period cancelation of two wave packets of large width.

One may be curious what happens for the wave packet dynamics when one of the Hermitian leads is removed and the system become semi-infinite. To answer this question, we apply the above analysis on this semi-infinite sandwich system. For the Hermitian lead, there are two zero energy channels of wave packets with opposite group velocities. In contrast, there is only one zero energy channel of wave packet, although it allows a wave packet propagating with two opposite group velocities. A coalescing

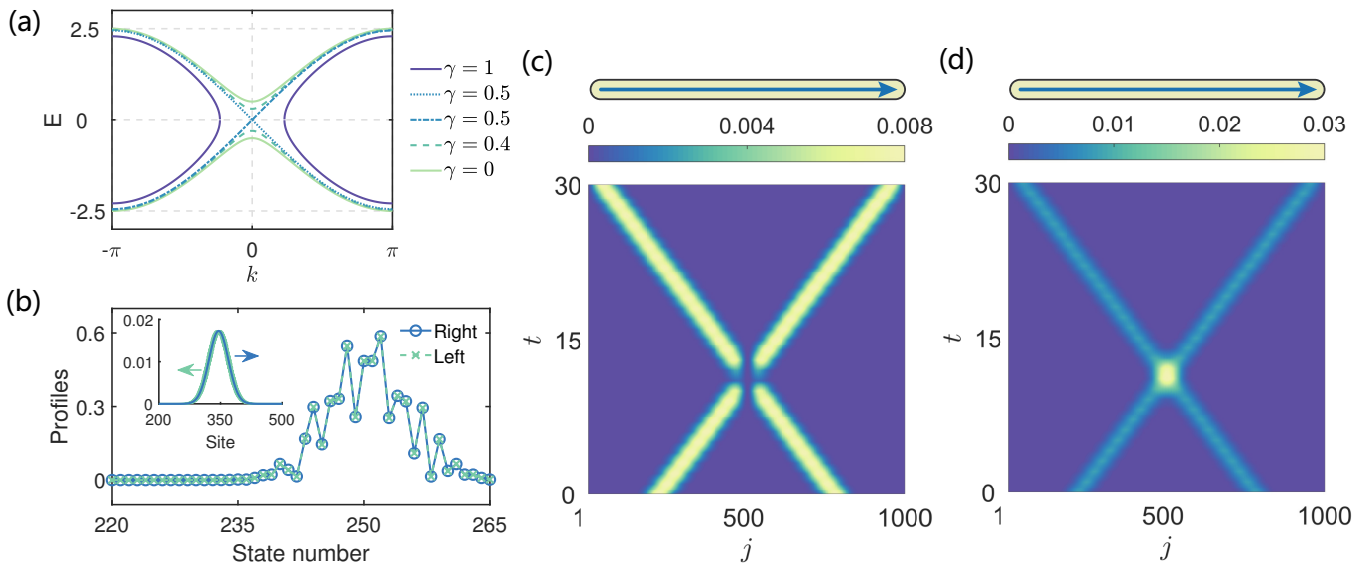


FIG. 5. (a) Energy dispersion of the non-Hermitian SSH ring in Eq. (9) for several typical value of γ when $J = 1$ and $\delta = 0.5$. Here the energy is in unit of J . (b) Profiles of two wave packets ($|\psi_L\rangle$ and $|\psi_R\rangle$) with opposite group velocities in k space and real space (inset figure). Here the state number represents the number of eigen states sorted by the energy from small to large. The size of the chain system is $N = 500$, and other parameters are $J = 1$, $\delta = 0.5$ and $\gamma = 0.5$. (c) and (d) are the numerical simulations of wave packet dynamics in the non-Hermitian SSH chain with the initial states: (c) $(|\psi_L\rangle + |\psi_R\rangle)/\sqrt{2}$, and (d) $(|\psi_L\rangle - |\psi_R\rangle)/\sqrt{2}$. The size of the system is $N = 1000$, and other parameters are $J = 1$, $\delta = 0.5$ and $\gamma = 0.5$. The time unit is $10J^{-1}$.

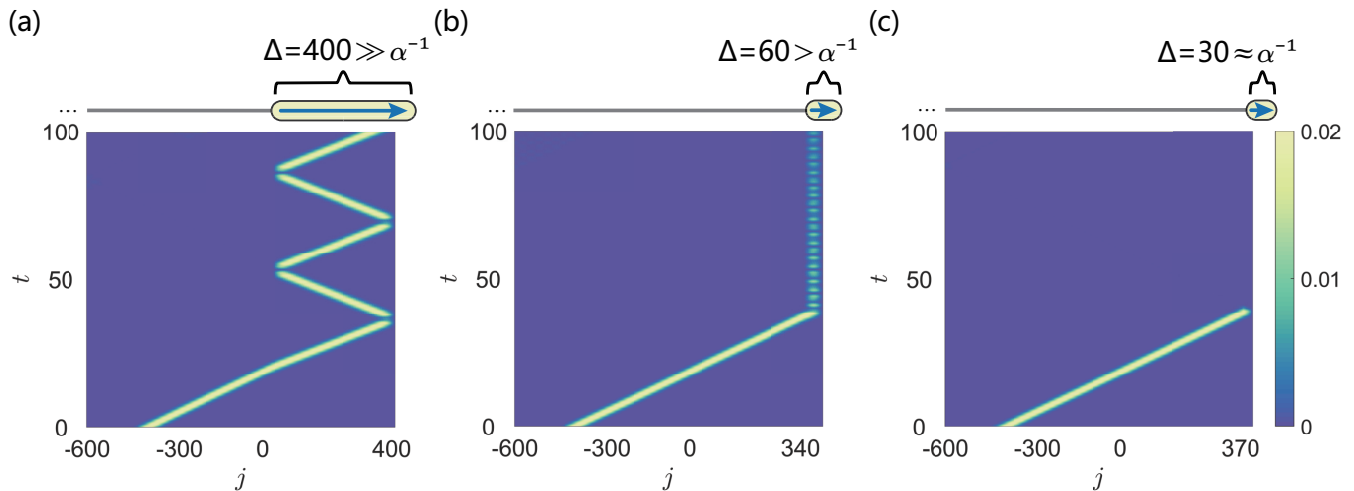


FIG. 6. Numerical simulations of the dynamics for the semi-infinite system, which consists of a uniform semi-infinite chain and a non-Hermitian SSH segment. (a) Coherent confinement when the width of the wave packet is much smaller than the size of the segment. (b) When the width of the wave packet approaches the size of the segment, the confined probability decreases. (c) Perfectly absorbed when the width of the wave packet is approximately equal to the size of the segment. The parameters of the initial excitation are $\alpha = 0.04$, $N_c = -400$ and $k_c = -\pi/2$; and for the system are $J = 1$, $\delta = 0.5$ and $\gamma = 0.5$. The time unit is $10J^{-1}$.

wave packet in the SSH segment cannot escape via the lead through which it comes. Thus once a wave packet comes into the SSH segment as perfect transmission, it bounces up and down within the segment. Furthermore, the Dirac probability within the segment is periodic due to the interference effect between incident and reflected

parts of the wave packet at boundaries.

To verify the above predictions, we perform the numerical simulation for the evolution of a Gaussian wave packet in the form of Eq. (8). The numerical results are shown in Fig. 6. In Fig. 6(a), the size of the segment is $\Delta = 400$. We can see that when the width of the wave

packet is much smaller than the size of the non-Hermitian SSH segment, the wave packet is confined in the segment. Figure 6(b) show that when the width of the wave packet approaches to the size of the segment $\Delta = 60$, the confined probability is reduced. In Fig. 6(c), the size of the segment is $\Delta = 30$. We can see the when the width of the wave packet approximate equal to the size of the segment $\Delta \approx \alpha^{-1} = 25$, the wave packet is perfectly absorbed. These results accords with our predictions.

V. SUMMARY

In summary, we have studied wave packet dynamics in the compound system which consists of a non-Hermitian SSH segment and a Hermitian uniform chain. Both systems support left and right propagating wave packets with zero energy. However, two wave packets in the former are quasi-coalescing, matching only one of two channels (left or right) in the Hermitian chain. This leads to unidirectional dynamics at the interface of the two subsystems. A wave packet in an SSH segment embedded in a uniform chain (a sandwich structure) is either perfectly transmitted or totally reflected at the interface, depending on the direction of the SSH segment. In addition, two quasi-coalescing wave packets interfere with each other constructively or destructively when they meet together. These result in peculiar phenomena which are exclusive in non-Hermitian systems: For a sandwich structure, an incident wave packet is either allowed perfect transmission or stimulates an amplified reflecting wave train with the length proportional to the size of the SSH segment. In addition, for a Hermitian-non-Hermitian junction system, an incident wave packet can be well confined in or perfectly absorbed by the SSH segment, depending on the length of the SSH segment. The model setup contains only staggered tunneling strength and imaginary potentials, which has relative simple geometrical structure and non-Hermitian components. It should be experimentally accessible in optical system [4, 44–46]. An inspired manifestation is the unidirectional invisibility of Bragg scatterers for the simulation of multi-embedded-SSH-segment system. Our findings are applicable to the schemes of realizing quantum state storage, quantum diode and lasing device.

APPENDIX

In this Appendix, we present the derivations of (A) the scattering solutions of the Hamiltonian in Eq. (1); (B) the zero energy solution for semi-infinite SSH chain; (C) and (D) the analysis for the solution of SSH ring, introducing a concept of quasi-coalescing energy level sets.

A. The scattering solutions of \mathcal{H}

The Bethe ansatz wave function of a scattering state $|\psi\rangle$ takes the form

$$|\psi\rangle = \sum_{j=-\infty}^{\infty} f_j |j\rangle. \quad (\text{A1})$$

with

$$f_j = \begin{cases} \mathcal{I}e^{iKj} + \mathcal{O}e^{-iKj}, & j < 0 \\ \mathcal{I}^A e^{-ikj} + \mathcal{O}^A e^{ikj}, & j = 2l \\ \mathcal{I}^B e^{-ikj} + \mathcal{O}^B e^{ikj}, & j = 2l + 1 \end{cases}. \quad (\text{A2})$$

Here $l = 0, 1, 2, \dots$. The Schrödinger equation $\mathcal{H}|\psi\rangle = E|\psi\rangle$ gives the expression of energy

$$E = 2J \cos K \quad (\text{A3}) \\ = \pm \sqrt{J^2 - \gamma^2 + (1 + \delta)^2 + 2J(1 + \delta) \cos(2k)},$$

and the equations for \mathcal{I} , \mathcal{O} , $\mathcal{I}^{A/B}$, and $\mathcal{O}^{A/B}$

$$\begin{aligned} -\nu_{-K}\mathcal{O} + J\mathcal{O}^A &= \nu_K\mathcal{I} - J\mathcal{I}^A, \\ J e^{iK}\mathcal{O} - \mu_{-k}\mathcal{O}^A &= -J e^{-iK}\mathcal{I} + \mu_k\mathcal{I}^A, \\ \mathcal{I}^B &= \lambda_k\mathcal{I}^A, \\ \mathcal{O}^B &= \lambda_{-k}\mathcal{O}^A, \end{aligned} \quad (\text{A4})$$

in which,

$$\begin{aligned} \mu_k &= (E - i\gamma) - (1 + \delta) \lambda_k e^{-ik}, \\ \nu_K &= E e^{-iK} - J e^{-2iK}, \\ \lambda_k &= \frac{J e^{-ik} + (1 + \delta) e^{ik}}{E + i\gamma}. \end{aligned} \quad (\text{A5})$$

When $\gamma = (1 + \delta - J)$, the energy has the simple form

$$E = 2J \cos K = 2\sqrt{J(1 + \delta)} \cos k. \quad (\text{A6})$$

We consider the solutions with zero energy. Equation $E = 0$ gives four solutions for K and k , that is $(K, k) = (-\pi/2, -\pi/2)$, $(\pi/2, \pi/2)$, $(\pi/2, -\pi/2)$, $(-\pi/2, \pi/2)$. However, it can be check that they correspond to the same wave function

$$|\psi\rangle = \sum_{j=-\infty}^{\infty} e^{-i\frac{\pi}{2}j} |j\rangle, \quad (\text{A7})$$

The Hamiltonian fulfill $\mathcal{H}^\dagger = \mathcal{H}^*$, thus the eigenstate with zero energy for \mathcal{H}^\dagger is

$$|\tilde{\psi}\rangle = |\psi\rangle^* = \sum_{j=-\infty}^{\infty} e^{i\frac{\pi}{2}j} |j\rangle, \quad (\text{A8})$$

For the present model, it is tough to get the complete solutions analytically. Here we provide the complete solution for the finite system consisted of two subsystems (the uniform chain and the non-Hermitian SSH chain) by performing numerically exact diagonalization to clarify that

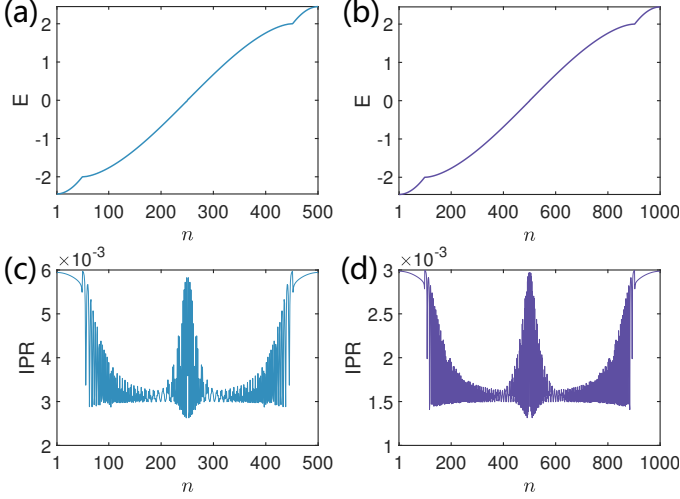


FIG. A1. (a) and (b) are the energy spectra for the finite system obtained by numerical diagonalization. (c) and (d) are the IPR corresponding to (a) and (b), respectively. The size of system is $250 + 250$ for (a) and (c); and is $500 + 500$ for (b) and (d). Other parameters are $J = 1$, $\delta = 0.5$ and $\gamma = 0.5$. Here the energy is in unit of J .

the energy spectrum is real and all the eigenstates are not bound states. We introduce the inverse participation ratio (IPR), which is defined as $\text{IPR}(n) = \sum_j |\langle j | \psi_n \rangle|^4$, with n denotes the state number and j denotes the lattice site, and the eigenstates $|\psi_n\rangle$ are Dirac normalized. In Fig. A1, we plot the energy spectrum and the corresponding IPR with different lattice size. We observe that all the eigenstates of the finite system has real eigen energy. The IPR are finite and decay when the size of the system increase, which indicates that all the eigen states are not bound states for a system with large lattice size.

B. Zero energy solution of the semi-infinite SSH chain

The ansatz wave function for the the semi-infinite SSH chain in Eq. (3) takes the form

$$|\psi_k\rangle = \sum_{j=0}^{\infty} f_j |j\rangle, \quad (\text{A9})$$

with

$$f_j = \begin{cases} \mathcal{I}^A e^{-ikj} + \mathcal{O}^A e^{ikj}, & j = 2l \\ \mathcal{I}^B e^{-ikj} + \mathcal{O}^B e^{ikj}, & j = 2l + 1 \end{cases}, \quad (\text{A10})$$

The Schrödinger equation $H_{\text{II}} |\psi_k\rangle = E_k |\psi_k\rangle$ gives

$$(1 + \delta) (\mathcal{I}^B e^{-ik} + \mathcal{O}^B e^{ik}) + (i\gamma - E_k) (\mathcal{I}^A + \mathcal{O}^A) = 0, \quad (\text{A11})$$

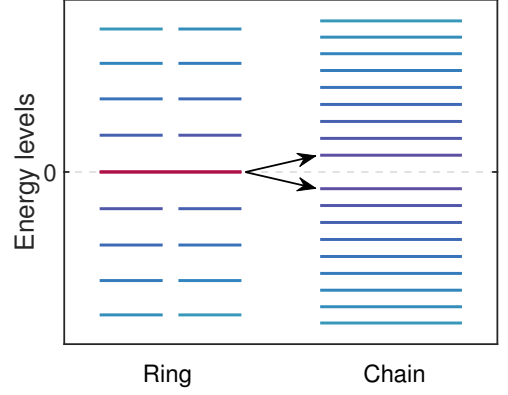


FIG. A2. Schematic illustration of the energy levels of the non-Hermitian SSH model at EP with periodic and open boundary (by breaking one of the weak hopping term) conditions, respectively. For a ring system, zero-level coalescence is split into two levels when the open boundary condition is imposed.

and

$$\begin{aligned} [i\gamma - E_k] \mathcal{I}^A + [(1 + \delta) e^{-ik} + J e^{ik}] \mathcal{I}^B &= 0, \\ [J e^{-ik} + (1 + \delta) e^{ik}] \mathcal{I}^A + [-i\gamma - E_k] \mathcal{I}^B &= 0, \\ [i\gamma - E_k] \mathcal{O}^A + [(1 + \delta) e^{ik} + J e^{-ik}] \mathcal{O}^B &= 0, \\ [J e^{ik} + (1 + \delta) e^{-ik}] \mathcal{O}^A + [-i\gamma - E_k] \mathcal{O}^B &= 0 \end{aligned} \quad (\text{A12})$$

Conditions for the existence of nonzero solutions are

$$\begin{vmatrix} i\gamma - E_k & (1 + \delta) e^{-ik} + J e^{ik} \\ J e^{-ik} + (1 + \delta) e^{ik} & -i\gamma - E_k \end{vmatrix} = 0, \quad (\text{A13})$$

and

$$\begin{vmatrix} i\gamma - E_k & (1 + \delta) e^{ik} + J e^{-ik} \\ J e^{ik} + (1 + \delta) e^{-ik} & -i\gamma - E_k \end{vmatrix} = 0, \quad (\text{A14})$$

which both give

$$E_k = \pm \sqrt{J^2 - \gamma^2 + (1 + \delta)^2 + 2J(1 + \delta) \cos(2k)}. \quad (\text{A15})$$

On the other hand, from Eqs. (A11) and (A12), we obtain

$$\begin{aligned} \mathcal{I}^B &= \frac{(E_k - i\gamma) e^{ik}}{1 + \delta + J e^{2ik}}, \\ \mathcal{O}^A &= -\frac{[(1 + \delta) e^{2ik} + J] e^{2ik}}{1 + \delta + J e^{2ik}}, \\ \mathcal{O}^B &= -\frac{(E_k - i\gamma) e^{3ik}}{1 + \delta + J e^{2ik}}. \end{aligned} \quad (\text{A16})$$

Here we set $\mathcal{I}^A = 1$.

We are looking for the solution with zero energy under the parameter $\gamma = \pm(1 + \delta - J)$. Eq. (A15) is reduced to $E_k = 2\sqrt{J(1 + \delta)} \cos k = 0$, which requires $k = \pm\pi/2$. Substitute $\gamma = \pm(1 + \delta - J)$ and $k = \pm\pi/2$ into Eqs. (A10) and (A16), we have

$$f_j = \begin{cases} \pm (e^{-i\frac{\pi}{2}j} - e^{i\frac{\pi}{2}j}), & j = 2l \\ \pm (e^{-i\frac{\pi}{2}j} + e^{i\frac{\pi}{2}j}), & j = 2l + 1 \end{cases}. \quad (\text{A17})$$

f_j is zero because $l = 0, 1, 2, \dots$, which means that the zero energy solution is forbidden. This can be seen from the spectrum of the SSH chain in Ref. [37, 40]. We demonstrate this point in Fig. A2 by comparison two energy level structures of SSH model with open and periodic boundary conditions. We see that the coalescing level with zero energy in SSH ring disappears when the open boundary condition is imposed. It accords with the vanishing zero energy solution for semi-infinite SSH chain since the solution for an open chain can be obtained by matching the solutions from two semi-infinite chains.

C. Hermitian dynamics in a SSH ring

For the purpose of explaining the Hermitian dynamics in the current non-Hermitian system, we consider a solvable non-Hermitian SSH ring with the Hamiltonian

$$H_{\text{Ring}} = \sum_{l=1}^N [(1 + \delta) a_{2l-1}^\dagger a_{2l} + J a_{2l}^\dagger a_{2l+1} + \text{H.c.} + i\gamma (a_{2l-1}^\dagger a_{2l-1} - a_{2l}^\dagger a_{2l})]. \quad (\text{A18})$$

In the \mathcal{PT} -symmetric region which support real eigen energy, the Hamiltonian can be diagonalized as

$$H_{\text{Ring}} = \sum_k (\varepsilon_k^+ \bar{\alpha}_{k,+} \alpha_{k,+} + \varepsilon_k^- \bar{\alpha}_{k,-} \alpha_{k,-}), \quad (\text{A19})$$

with the eigen energy

$$\begin{aligned} \varepsilon_k^\pm &= \pm \sqrt{g_k g_k^* - \gamma^2} \\ &= \pm \sqrt{J^2 + (1 + \delta)^2 - 2J(1 + \delta) \cos k - \gamma^2} \end{aligned} \quad (\text{A20})$$

by taking the linear transformation

$$\bar{\alpha}_{k,\pm} = \frac{1}{\sqrt{2}} \left(\pm e^{i\theta_k^\pm} \sqrt{\frac{g_k}{g_k^*}} a_{k,1}^\dagger + a_{k,0}^\dagger \right), \quad (\text{A21})$$

$$\alpha_{k,\pm} = \frac{\sqrt{2}}{e^{i\theta_k^+} + e^{i\theta_k^-}} \left(\sqrt{\frac{g_k^*}{g_k}} a_{k,1} + e^{-i\theta_k^\pm} a_{k,0} \right), \quad (\text{A22})$$

where

$$\begin{aligned} a_{k,\lambda} &= N^{-1/2} \sum_{l=1}^N e^{i(k+\pi)l} a_{2l-\lambda}, \quad (\lambda = 1, 0), \\ e^{i\theta_k^\pm} &= \frac{\pm \sqrt{g_k g_k^* - \gamma^2} + i\gamma}{\pm \sqrt{g_k g_k^*}}, \\ g_k &= (1 + \delta) - J e^{ik}. \end{aligned} \quad (\text{A23})$$

It can be checked that operators $\bar{\alpha}_{k,\pm}$ satisfy the quasi-canonical commutation relations

$$\begin{aligned} [\bar{\alpha}_{k,+}^\dagger, \bar{\alpha}_{k',+}]_\pm &= [\bar{\alpha}_{k,-}^\dagger, \bar{\alpha}_{k',-}]_\pm = \delta_{kk'}, \\ [\bar{\alpha}_{k,+}^\dagger, \bar{\alpha}_{k',-}]_\pm &= 2ie^{-i\theta_k^\pm} \sin \theta_k^\pm \delta_{kk'}. \end{aligned} \quad (\text{A24})$$

Here $[\cdot, \cdot]_\pm$ denotes the the commutator and anticommutator.

Now we consider the time evolution of an arbitrary initial state

$$|\psi(0)\rangle = \sum_k (C_{k,+} \bar{\alpha}_{k,+} + C_{k,-} \bar{\alpha}_{k,-}) |\text{vac}\rangle. \quad (\text{A25})$$

At instant t , we have

$$\begin{aligned} |\psi(t)\rangle &= e^{-iHt} |\psi(0)\rangle \\ &= \sum_k \left(e^{-i\varepsilon_k^+ t} C_{k,+} \bar{\alpha}_{k,+} + e^{-i\varepsilon_k^- t} C_{k,-} \bar{\alpha}_{k,-} \right) |\text{vac}\rangle. \end{aligned} \quad (\text{A26})$$

Using the quasicanonical commutation relations of Eqs. (A24), the Dirac probability can be written as

$$\begin{aligned} P(t) &= \langle \psi(t) | \psi(t) \rangle \\ &= \sum_k \left(|C_{k,+}|^2 + |C_{k,-}|^2 \right) \\ &\quad + 4 \sum_k \text{Re} \left(-ie^{i\theta_k^+} e^{-2i\varepsilon_k^+ t} C_{k,+} C_{k,-}^* \right) \sin \theta_k^+. \end{aligned} \quad (\text{A27})$$

It indicate that when the initial states are structured properly: $C_{k,+} C_{k,-}^* \rightarrow 0$ (the initial state does not involve components of $\bar{\alpha}_{k,+}$ and $\bar{\alpha}_{k,-}$ simultaneously), the Dirac probability conserve.

D. Quasi-coalescing levels in a SSH ring

We consider a non-Hermitian SSH ring with the Hamiltonian of Eq. (A18). According to the analysis in Appendix C, the eigenstates of two bands ε_k^\pm can be obtained

$$\begin{aligned} |\psi_k^\pm\rangle &= \bar{\alpha}_{k,\pm} |\text{vac}\rangle \\ &= \frac{1}{\sqrt{2}} \left(\frac{\varepsilon_k^\pm + i\gamma}{1 + \delta - J e^{-ik}} a_{k,1}^\dagger + a_{k,0}^\dagger \right) |\text{vac}\rangle \end{aligned} \quad (\text{A28})$$

Here the wave functions are Dirac normalized. We are interested in the overlap between the corresponding wave functions of two bands, which is defined as

$$O_k = |\langle \psi_k^+ | \psi_k^- \rangle|. \quad (\text{A29})$$

Direct derivation shows that

$$O_k = \frac{|\gamma|}{\sqrt{J^2 + (1 + \delta)^2 - 2J(1 + \delta) \cos k}}. \quad (\text{A30})$$

At EP with $\gamma = (1 + \delta - J)$, we note that $O_{k=0} = 1$ indicating the coalescence of state. We also find that $O_k \approx 1$ for small k , especially in the case of large γ , which corresponds to strong dimerization limit. Actually, taking $\gamma = (1 + \delta - J)$ and $\cos k \approx 1 - k^2/2$, we have

$$O_k \approx \frac{1}{\sqrt{1 + J(1 + \delta) k^2 / \gamma^2}}, \quad (\text{A31})$$

which approaches to 1 for large γ . We plot Eq. (A30) for several typical γ in Fig. A3 to demonstrate this point. We conclude that there exist two sets of energy levels near the zero point, which are quasi-coalescing. This is directly related to the vanishing zero energy solution in SSH chain we discussed in the Appendix B.

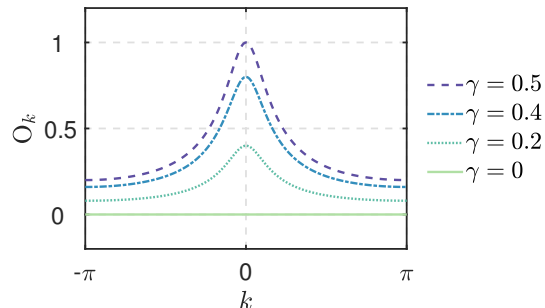


FIG. A3. The overlap between the corresponding wave functions of two bands of the non-Hermitian SSH ring for several typical γ . Other parameters are $J = 1$ and $\delta = 0.5$.

ACKNOWLEDGMENTS

This work was supported by National Natural Science Foundation of China (under Grant No. 11874225).

-
- [1] M. Kulishov, J. M. Laniel, N. Bélanger, J. Azaña, and D. V. Plant, *Opt. Express* **13**, 3068 (2005).
- [2] S. Longhi, Transparency in Bragg scattering and phase conjugation, *Opt. Lett.* **35**, 3844 (2010).
- [3] Z. Lin, H. Ramezani, T. Eichelkraut, T. Kottos, H. Cao, and D. N. Christodoulides, Unidirectional Invisibility Induced by PT-Symmetric Periodic Structures, *Phys. Rev. Lett.* **106**, 213901 (2011).
- [4] A. Regensburger, C. Bersch, M.-A. Miri, G. Onishchukov, D. N. Christodoulides, and U. Peschel, Parity-time synthetic photonic lattices, *Nature (London)* **488**, 167 (2012).
- [5] T. Eichelkraut, R. Heilmann, S. Weimann, S. Stützer, F. Dreisow, D. N. Christodoulides, S. Nolte, and A. Szameit, Mobility transition from ballistic to diffusive transport in non-Hermitian lattices, *Nat. Commun.* **4**, 2533 (2013).
- [6] B. Peng, Ş. K. Özdemir, F. Lei, F. Monifi, M. Gianfreda, G. L. Long, S. Fan, F. Nori, C. M. Bender, and L. Yang, Parity-time-symmetric whispering-gallery microcavities, *Nat. Phys.* **10**, 394 (2014).
- [7] L. Chang, X. Jiang, S. Hua, C. Yang, J. Wen, L. Jiang, G. Li, G. Wang, and M. Xiao, Parity-time symmetry and variable optical isolation in active-passive-coupled microresonators, *Nat. Photonics* **8**, 524 (2014).
- [8] L. Feng, Y.-L. Xu, W. S. Fegadolli, M.-H. Lu, J. E. B. Oliveira, V. R. Almeida, Y.-F. Chen, and A. Scherer, Experimental demonstration of a unidirectional reflectionless parity-time metamaterial at optical frequencies, *Nat. Mater.* **12**, 108 (2013).
- [9] S. Longhi, Invisibility in non-Hermitian tight-binding lattices, *Phys. Rev. A* **82**, 032111 (2010).
- [10] S. Longhi, and G. Della Valle, Invisible defects in complex crystals, *Ann. Phys. (NY)* **334**, 35 (2013).
- [11] X. Z. Zhang, and Z. Song, Momentum-independent reflectionless transmission in the non-Hermitian time-reversal symmetric system, *Ann. Phys. (NY)* **339**, 109 (2013).
- [12] Y. Sun, W. Tan, H. Q. Li, J. Li, and H. Chen, Experimental Demonstration of a Coherent Perfect Absorber with PT Phase Transition, *Phys. Rev. Lett.* **112**, 143903 (2014).
- [13] A. Mostafazadeh, Spectral Singularities of Complex Scattering Potentials and Infinite Reflection and Transmission Coefficients at Real Energies, *Phys. Rev. Lett.* **102**, 220402 (2009).
- [14] S. Longhi, Spectral singularities in a non-Hermitian Friedrichs-Fano-Anderson model, *Phys. Rev. B* **80**, 165125 (2009).
- [15] X. Z. Zhang, L. Jin, and Z. Song, Self-sustained emission in semi-infinite non-Hermitian systems at the exceptional point, *Phys. Rev. A* **87**, 042118 (2013).
- [16] S. Longhi, Half-spectral unidirectional invisibility in non-Hermitian periodic optical structures, *Opt. Lett.* **40**, 5694 (2015).
- [17] X. Q. Li, X. Z. Zhang, G. Zhang, and Z. Song, Asymmetric transmission through a flux-controlled non-Hermitian scattering center, *Phys. Rev. A* **91**, 032101 (2015).
- [18] B. Peng, Ş. K. Özdemir, S. Rotter, H. Yilmaz, M. Liertzer, F. Monifi, C. M. Bender, F. Nori, and L. Yang, Loss-induced suppression and revival of lasing, *Science* **346**, 328 (2014).
- [19] L. Feng, Z. J. Wong, R. -M. Ma, Y. Wang, and X. Zhang, Single-mode laser by parity-time symmetry breaking, *Science* **346**, 972 (2014).
- [20] H. Hodaei, M.-A. Miri, M. Heinrich, D. N. Christodoulides, and M. Khajavikhan, Parity-time-symmetric microring lasers, *Science* **346**, 975 (2014).
- [21] T. E. Lee, F. Reiter, and N. Moiseyev, Entanglement and Spin Squeezing in Non-Hermitian Phase Transitions, *Phys. Rev. Lett.* **113**, 250401 (2014).
- [22] T. E. Lee, and C. K. Chan, Heralded Magnetism in Non-Hermitian Atomic Systems, *Phys. Rev. X* **4**, 041001 (2014).
- [23] C. Li, and Z. Song, Generation of Bell, W, and Greenberger-Horne-Zeilinger states via exceptional points in non-Hermitian quantum spin systems, *Phys. Rev. A* **91**, 062104 (2015).
- [24] S. Lin, X. Z. Zhang, C. Li, and Z. Song, Long-range entangled zero-mode state in a non-Hermitian lattice, *Phys. Rev. A* **94**, 042133 (2016).

- [25] M. F. Yanik and S. Fan, Stopping Light All Optically, *Phys. Rev. Lett.* **92**, 083901 (2004).
- [26] M. F. Yanik and S. Fan, Time Reversal of Light with Linear Optics and Modulators, *Phys. Rev. Lett.* **93**, 173903 (2004).
- [27] S. Longhi, Stopping and time reversal of light in dynamic photonic structures via Bloch oscillations, *Phys. Rev. E* **75**, 026606 (2007);
- [28] W. H. Hu, L. Jin, and Z. Song, Dynamics of one-dimensional tight-binding models with arbitrary time-dependent external homogeneous fields, *Quantum Inf. Process* **12**, 3569 (2013).
- [29] S. Longhi, Non-reciprocal transmission in photonic lattices based on unidirectional coherent perfect absorption, *Opt. Lett.* **40**, 1278 (2015).
- [30] L. Jin, X. Z. Zhang, G. Zhang, and Z. Song, Reciprocal and unidirectional scattering of parity-time symmetric structures, *Sci. Rep.* **6**, 20976 (2016).
- [31] L. Jin, P. Wang, and Z. Song, Unidirectional perfect absorber, *Sci. Rep.* **6**, 32919 (2016).
- [32] C. Li, L. Jin, and Z. Song, Non-Hermitian interferometer: Unidirectional amplification without distortion, *Phys. Rev. A* **95**, 022125 (2017).
- [33] L. Jin, P. Wang, and Z. Song, One-way light transport controlled by synthetic magnetic fluxes and-symmetric resonators, *New J. Phys.* **19**, 015010 (2017).
- [34] L. Jin and Z. Song, Incident Direction Independent Wave Propagation and Unidirectional Lasing, *Phys. Rev. Lett.* **121**, 073901 (2018).
- [35] X. Z. Zhang and Z. Song, Partial topological Zak phase and dynamical confinement in a non-Hermitian bipartite system, *Phys. Rev. A* **99**, 012113 (2019).
- [36] K. L. Zhang, L. Jin, and Z. Song, Helical resonant transport and purified amplification at an exceptional point, *Phys. Rev. B* **100**, 144301 (2019).
- [37] K. L. Zhang, P. Wang, and Z. Song, Exceptional-point-induced lasing dynamics in a non-Hermitian Su-Schrieffer-Heeger model, *Phys. Rev. A* **99**, 042111 (2019).
- [38] F. Bloch, Bemerkung zur Elektronentheorie des Ferromagnetismus und der elektrischen Leitfähigkeit, *Z. Phys.* **57**, 545 (1929).
- [39] C. Zener, A theory of the electrical breakdown of solid dielectrics, *Proc. R. Soc. London A* **145**, 523 (1934).
- [40] K. L. Zhang, P. Wang, G. Zhang, and Z. Song, Simple harmonic oscillation in a non-Hermitian Su-Schrieffer-Heeger chain at the exceptional point, *Phys. Rev. A* **98**, 022128 (2018).
- [41] L. Jin and Z. Song, Hermitian dynamics in a class of pseudo-Hermitian networks, *Phys. Rev. A* **84**, 042116 (2011).
- [42] W. H. Hu, L. Jin, Y. Li, and Z. Song, Probability-preserving evolution in a non-Hermitian two-band model, *Phys. Rev. A* **86**, 042110 (2012).
- [43] K. L. Zhang, X. M. Yang, and Z. Song, Quantum transport in non-Hermitian impurity arrays, *Phys. Rev. B* **100**, 024305 (2019).
- [44] S. Weimann, M. Kremer, Y. Plotnik, Y. Lumer, S. Nolte, K. G. Makris, M. Segev, M. C. Rechtsman, and A. Szameit, Topologically Protected Bound States in Photonic Parity-Time-Symmetric Crystals, *Nat. Mater.* **16**, 433 (2017).
- [45] H. Zhao, P. Miao, M. H. Teimourpour, S. Malzard, R. El-Ganainy, H. Schomerus, and L. Feng, Topological hybrid silicon microlasers, *Nat. Commun.* **9**, 981 (2018).
- [46] M. Pan, H. Zhao, P. Miao, S. Longhi, and L. Feng, Photonic zero mode in a non-Hermitian photonic lattice, *Nat. Commun.* **9**, 1308 (2018).